INTERNATIONAL JOURNAL FOR NUMERICAL METHODS IN FLUIDS, VOL. 19, 377–393 (1994)

NUMERICAL SIMULATION OF A LOW-REYNOLDS-NUMBER TURBULENT WAKE BEHIND A FLAT PLATE

PETER R.VOKE

Department of Mechanical Engineering, The University of Surrey, Guildford GU2 5XH, U.K.

AND

SOCRATES G. POTAMITIS

Department of Computer Science, The Philips College, PO Box 8008, Nicosia, Cyprus

SUMMARY

A numerical simulation of a plane turbulent wake at a very low Reynolds number has been performed using finite volume methods. The wake was produced by allowing two turbulent boundary layers, simulated separately in advance, to interact downstream of the trailing edge of a thin flat plate. A number of innovative numerical techniques were required in the simulation, such as the provision of fully turbulent time-dependent inflow data from a separate simulation, advective outflow boundary conditions and the approximate representation of an internal solid surface by a method which is computationally efficient. The resulting simulation successfully reproduced many of the statistical properties of the turbulent near-wake flow at low Reynolds number.

KEY WORDS Turbulence Numerical simulation Wake

1. INTRODUCTION

The direct or large-eddy simulation of the turbulent wake is a demanding but useful exercise, since it allows the detailed study of a flow in which rapid streamwise adjustment is present in a turbulent flow. For this reason the near-wake region, which is critical for the prediction of wing lift, is difficult to model theoretically. The simulation of a turbulent wake demands a number of developments in the technique of large-eddy simulation. The flow is spatially developing and has a strong cross-stream inhomogeneity, so that only the spanwise dimension can be treated as statistically homogeneous. Time-dependent turbulent inflow and outflow boundary conditions are required and it is vital to allow the very-near-wake region to influence the region upstream of the trailing edge through the pressure field.

We have simulated the simplest wake, that behind a flat plate with statistically identical boundary layers on either side. The flow is incompressible, in contrast with existing simulations by Chen *et al.*,[1] Lele[2] and Compte *et al.*,[3] who have studied transition in compressible wakes. The geometry of our computation is shown in Figure 1. The simplicity of the geometry has allowed a fast method to be developed for the simulation of the flow in the U-shaped region around the trailing edge. The numerical methods employed for the present simulation are based on those originally proposed by Lilly[4] on the basis of Arakawa's[5] concepts. In this approach a

CCC 0271–2091/94/170377–17

Received July 1993
Revised February 1994

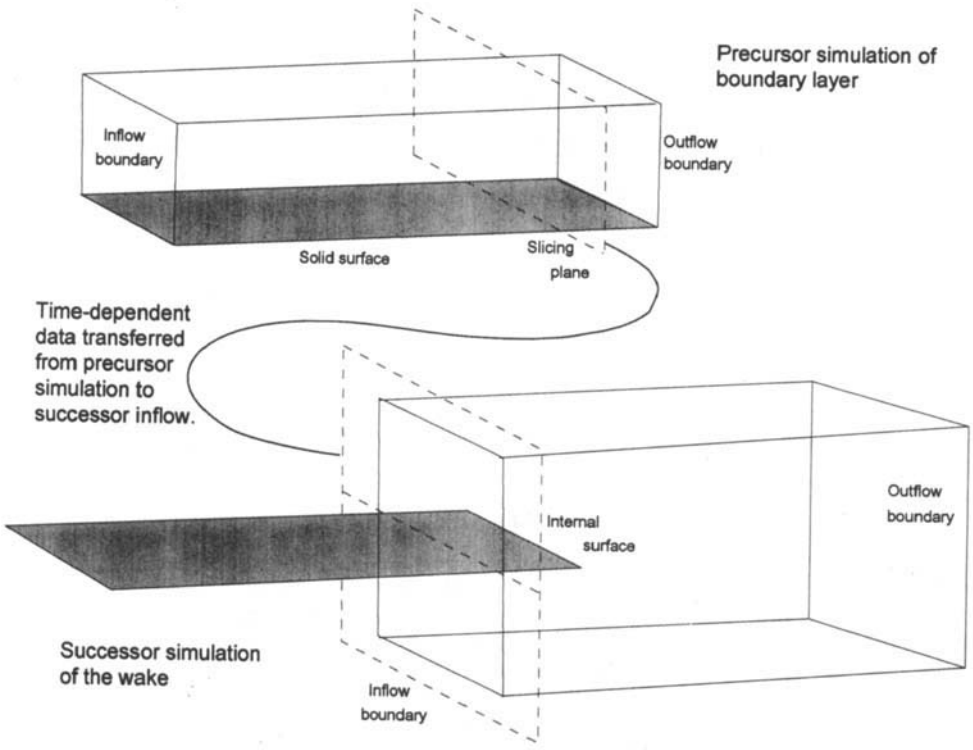

Figure 1. Geometry of the boundary layer (precursor) and near-wake (successor) simulations

linear finite volume scheme is devised that has the property of conserving all components (u_1^2, u_2^2, u_3^2) of the kinetic energy, and hence also the total kinetic energy, in the discretization of the advection term of the Navier–Stokes equations. It is thus impossible for energy to be created or destroyed by dissipative errors in this term, in spite of the formally low order of the interpolations. Dispersive errors are present, however, and the fourth-order error in the discretization of the viscous term can also dissipate energy artificially.

Bryan[6] showed that the method could be extended straighforwardly to stretched meshes in three dimensions. Following application of similar techniques to simulations of meteorological flows by Smagorinsky[7] and others, Deardorff[8] set up the first true large-eddy simulation of a channel flow. The pivotal work of Schumann,[9] who gave the fullest description of the numerical method we employ here, has led to finite volume techniques being applied in numerous large-eddy simulation studies, such as those by Grötzbach,[10] Mason,[11] Klein and Friedrich,[12] Gao *et al.*[13] and others. At the highest resolutions currently practical (and provided that the Reynolds or Rayleigh numbers are low enough) it is possible to omit the subgrid-scale model from the computation: Gertz *et al.*[14] and Gavrilakis[15] have used finite volume methods in their direct numerical simulations of very different turbulent flows.

The discretization is performed on a staggered mesh, with stretching employed in both streamwise (x) and wall-normal (y) dimensions. The stretching must be gentle (the ratio of adjacent cell widths below 1·1) in order to avoid compromising the second-order accuracy of the scheme. The form of interpolation not only conserves mass and momentum volume-by-volume, but also conserves the squares of the velocity components in the advection term. The

linear differencing leads to a very simple seven-point pressure star which can be solved efficiently by vectorizing direct solvers.

2. METHODS

2.1. Finite volumes

The code is a finite volume discretization of the incompressible Navier–Stokes equations in conservative form,

$$\frac{\partial u_i}{\partial t} = -\frac{\partial p}{\partial x_i} + H_i, \tag{1}$$

where

$$H_i = \frac{\partial}{\partial x_j}\left[-u_i u_j + \nu\left(\frac{\partial u_i}{\partial x_j} + \frac{\partial u_j}{\partial x_i}\right)\right]. \tag{2}$$

The time stepping used is second-order open Adams,

$$u_i^{n+1} = u_i^n + \Delta t\left(-\frac{\partial p}{\partial x_i} + \tfrac{3}{2}H_i^n - \tfrac{1}{2}H_i^{n-1}\right), \tag{3}$$

where the superscripts indicate the time step.

All terms in the momentum equations are treated explicitly, apart from the pressure term $\partial p/\partial x_i$. The pressure is unknown at the current step and is therefore omitted from the time advancement (3), resulting in the computation of a provisional velocity u_i^* which does not obey continuity but which is related to the true velocity u_i^{n+1} at the next time step through a decomposition into its divergence-free and irrotational parts.

$$u_i^* = u_i^{n+1} + \Delta t\,\frac{\partial p}{\partial x_i}. \tag{4}$$

Thus u_i^{n+1} is the projection of u_i^* into the subspace of divergence-free vector functions.

Taking the divergence of (4) and using the fact that the new velocity field u_i^{n+1} must be divergence-free, i.e.

$$\frac{\partial u_i^{n+1}}{\partial x_i} = 0, \tag{5}$$

we obtain the Poisson equation for the pressure field p,

$$\nabla^2 p = \frac{1}{\Delta t}\frac{\partial u_i^*}{\partial x_i} = R. \tag{6}$$

The solution to this equation in discrete form is unique, just as the solution of the analytical equation is unique, provided that the surface integral of u_i^* over the boundaries of the computational domain is zero. Note that the field p is neither p^{n+1} nor p^n, though to second order

$$p = \frac{p^{n+1} + p^n}{2} = \frac{3p^n - p^{n-1}}{2}. \tag{7}$$

To find p, equation (6) is Fourier transformed in z, decomposing into a set of elliptic equations of the form

$$\frac{\partial^2 \tilde{p}}{\partial x^2} + \frac{\partial^2 \tilde{p}}{\partial y^2} - K_z^2 \hat{p} = \tilde{R}. \tag{8}$$

Since the difference operator is used to compute z-derivatives of p in configuration space, rather than a true analytical derivative, the operator K_z is related to the Fourier wave number k_z by

$$K_z = 2 \sin(\pi k_z / N_z)/\Delta z. \tag{9}$$

These equations are solved by a vectorized cyclic reduction technique based on the algorithm of Schwarztrauber,[16] which allows for stretching of the mesh in both the x- and the y-direction provided that the domain and the mesh remain rectangular. The method is formally identical to that used by Gavrilakis,[15] though the boundary conditions are clearly very different. The efficiency of the pressure solution algorithm is vital to our simulation, as is the case for other large-eddy simulations. The pressure solution demanded 50% of the CPU time in our simulation; with a less efficient solver it is easy for this part of the computation to overwhelm the remaining explicit calculations and make LES impractical. It is for this reason that LES and DNS have till now been performed in relatively simple geometries only.

2.2. *Inflow boundary*

The code used in this study was originally developed for the simulation of turbulent flow through a square or rectangular duct and has been extensively proved in that context by Gavrilakis.[15] To simulate an open, spatially developing flow such as the wake, the solid walls of the duct were replaced by inflow, outflow and free-slip boundaries

The wake is formed from the interaction of flows which have developed upstream, in the present case turbulent boundary layers. To simulate such a flow numerically, fully turbulent inflow data are required which have been derived from a separate simulation, called the precursor simulation by Tsai *et al.*,[17] of a low-Reynolds-number turbulent boundary layer. The boundary layer simulation used was one similar to those of Yang and Voke,[18] though performed on a finer mesh. A Blasius layer at the inflow of this simulation was destabilized rapidly by superimposing pseudorandom numbers and developed the characteristics of a young turbulent boundary layer within the computational domain, while the pseudorandom 'free-stream turbulence' decayed steadily and acquired the characteristics of genuine turbulence.

At the inflow plane of the wake simulation the three velocity components were specified by reading one transverse plane (a slice) of velocity data from the boundary layer simulations at each time step. The net mass flux into the computational volume was thus fixed by the independent precursor simulation. The transverse velocities just outside the computational volume were also fixed from the slices of transferred data. The data were taken from a plane towards the downstream end of the precursor simulation where the flow is fully turbulent, but a safe distance upstream of the outflow boundary of the precursor simulation. The two separate and uncorrelated sets of velocity data needed to provide inflow conditions for the upper and lower halves of the wake simulation were taken from the same precursor simulation at well-separated times in it history, some $1609_0/u_\tau$ apart.

2.3. *Outflow boundary*

An outflow boundary should be passive, reflecting no energy back into the computation, but

precise non-reflecting boundary conditions are difficult to implement in a strongly time-dependent computation with a broad spectrum of waves present. Instead, we have implemented advective conditions similar to those recommended by Bottaro.[19] This boundary condition exhibits very satisfactory behaviour for the wake simulation and has been employed for other studies using our code by Yang and Voke,[20] Gao *et al.*[13] and Lo.[21] The flow field within a few cells of the outflow boundary itself should be treated with caution, but otherwise the outflow boundary condition appears to be entirely passive.

At the outflow plane the advective boundary condition takes the form

$$\frac{\partial u_i}{\partial t} + U_c \frac{\partial u_i}{\partial x} = 0. \tag{10}$$

The convecting velocity U_c is fixed at each time step by averaging the streamwise velocity over a transverse plane. The streamwise gradient is computed by a second-order upwind difference and used in an explicit Adams formula, since the outflow velocity must be fixed in advance of the pressure solution at each time step and no velocities from the current step are yet known:

$$u_i^{n+1} = u_i^n + \Delta t U_c \left(\frac{3}{2} \frac{\partial u_i^n}{\partial x} - \frac{1}{2} \frac{\partial u_i^{n-1}}{\partial x} \right). \tag{11}$$

Equation (11) does not guarantee that the inflow and outflow at a particular time step are equal, since the outflow velocity is fixed with reference to values at previous steps. Any imbalance between the net inflow U_{in} and outflow U_{out} passing through the boundaries of the computational volume produces a singular problem for the pressure solver. The outflow velocity is therefore factored uniformly over the outflow plane to ensure that its integral balances the integrated inflow:

$$u_1^{n+1} \leftarrow u_1^{n+1} \times \frac{U_{in}}{U_{out}}. \tag{12}$$

2.4. *Side boundaries*

At the side boundaries an impermeable free-slip condition was used which fixed the normal velocity v to zero but allowed the streamwise and spanwise velocities to take any values. The side boundaries were removed some distance from the principal region of interest by stretching the y-mesh. The side boundaries should also strictly allow some outflow or inflow to accommodate growth of or entrainment into the wake, with the amount of outflow or inflow through the side boundaries being determined by the requirement for a uniform pressure field in the far field. Although such side flows are of importance for the simulation of free jets[21] and are also useful in the simulation of boundary layers,[20] they were not incorporated in this simulation of the wake, since the mean pressure gradient induced is low.

2.5. *Pressure boundary conditions*

The simulation of the wake includes a portion of the trailing edge of the plate, so that the flow downstream of the trailing edge may influence the boundary layers before they reach the trailing edge. This is most important physically, but results in a technical problem. The cyclic reduction pressure solver can only deal with the solution of the Poisson or Helmholz equation on a rectangular domain, without internal boundary conditions: the boundary conditions are enforced on the rectangular exterior boundary only.

In the finite volume code the pressure is solved by Fourier transformation in the spanwise (z) direction, leaving a set of inhomogeneous Helmholz equations including one Poisson equation for the wave number $k_z = 0$. These equations are solved subject to the Neumann boundary condition

$$\frac{\partial p}{\partial n} = 0, \tag{13}$$

where n is the co-ordinate normal to the boundary. This boundary condition is artificial, since the pressure at the boundary adjusts itself to ensure that continuity is satisfied there, as elsewhere.[22] The normal derivative of the pressure is therefore fixed by the normal velocity specified at the boundary and the values of the physical force terms, advective and viscous, which in general are non-zero.

In practice, in a staggered mesh, finite volume code such as the one used for this study, the actual physical value of the normal pressure gradient is irrelevant; only the difference

$$u_n = u_n^* - \frac{\partial p}{\partial n} \tag{14}$$

is meaningful, since altering the value of u_n^* alters the source term for the pressure in the Poisson equation in a way that precisely compensates for the change in the boundary condition. The pressure solution is the same regardless of the values of u_n^* on the boundaries. The artificial boundary condition (13) is used to alter the solution star at the edge of the domain to reflect the special form of the continuity equation at the boundary and remove the pressure value at the point just outside the boundary from the computation entirely. Our approach to the pressure solution is therefore to impose the desired physical boundary condition appropriate for u_n on u_n^* before the divergence of u_n^* is computed. The pressure star is then altered at the boundary to incorporate the homogeneous Neumann condition (13). The normal pressure gradient is thus absent from the equations representing the finite difference Laplacian of p. This strategy is the most efficient since it means that the pressure solution proceeds in the same manner regardless of the type of boundary being treated. The normal velocity u_n is zero for a solid or impermeable stress-free boundary and non-zero for inflow or outflow boundaries, but the pressure solution algorithm remains unaltered.

2.6. The internal boundary

The accurate solution of the pressure field at each of the large number of time steps of the simulation is critical: in a geometry such as that shown in Figure 1, the pressure solution might be expected to dominate the computer time usage. We have been able to maintain the very high speed of the Fourier/cyclic reduction solver in spite of the presence of a section of the trailing edge in the wake simulation, by using an innovative approximation for the pressure boundary conditions at the plate surface.

The intruding trailing edge (or *internal surface*) interferes with the simple pressure solution strategy outlined in the preceding subsection. The velocity component normal to the internal surface must be zero and hence the source term of the pressure equation must be altered. The standard method of dealing with a problem such as this is by use of an influence matrix: the intruding internal surface is treated as a small perturbation to the linear pressure problem for the flow without the internal surface. Large-eddy simulations have been performed using this method by Klein and Friedrich.[12] The pressure equation is solved without the perturbation and

the influence matrix is then used to compute alterations to the original source terms depending linearly on the resulting pressure gradient at the position of the internal surface and on the external flows. The Poisson equation is then solved again, producing a solution with zero flow through the internal surface.

The technique has a disadvantage for our purpose. Apart from the expense of the matrix computations, which could be borne, the additional pressure solution to be performed at each time step adds a large overhead to the CPU time. Since an exactly zero mass flux through the internal surface was not vital to the aims of the simulation, an approximate technique was sought, having most of the advantages of the influence matrix method without the computational expense. In order to maintain the efficiency of the direct pressure solver, the boundary condition on the intruding trailing edge of the plate (known as the *internal surface*) must be approximate. The momentum conditions are maintained exactly, with stresses being computed just as at an external boundary, but the mass flux through the surface is not precisely zero.

The method devised uses the pressure gradient on either side of the plate at the previous time step as a first-order estimate of the appropriate value for u^* at the current step. Note that different values are stored for each side of the plate, even though it is of zero thickness: these values are then used to compute the pressure source field. The resulting pressure solution allows a small but non-zero mass flow through the plate, the normal velocity v having a random sign and being of order Δt compared with other local velocities. For the present simulation these velocities were always less than 1% of the values that occurred downstream of the plate and so less than 0·1% of U_e. Since these non-zero values were random, the time-averaged flux through the plate was extremely close to zero. Higher-order multistep methods for predicting the pressure gradient at the internal surface have been tested and were found to be unstable.

The chosen method only involves a tiny amount of additional storage and computation. The CPU time per step is virtually unaltered compared with solving the unmodified flow. All other boundary conditions at the internal surface are imposed just as at any other solid boundary, so that the momentum equations include stresses computed in the same way as they would be for an exact solution with $v = 0$ on the internal surface.

2.7. Stability limits

The time-stepping scheme is second-order open Adams, consistent with the accuracy of the spatial interpolation. The viscous terms as well as the advection terms are treated explicitly, leading to the presence of a viscous stability limit as well as a CFL limit on the time step. In practice, at the low Reynolds number being simulated, the CFL limit is the more pressing, though this can change if a subgrid-scale model is included in the calculation. In both the precursor and successor simulations the CFL limit was strictly adhered to. Precise matching of the meshes and time steps in the precursor and successor computational volumes was found not to be possible, since the CFL limit would quickly be violated in the successor simulation. This occurs because the very fine mesh needed in the boundary layer simulation extends past the trailing edge, out into the centre of the wake where significant cross-stream velocities build up.

The change in the physical conditions along the line of the solid surface as the flow moves past the trailing edge therefore gives rise directly to a numerical problem. The simplest solution is to decrease the time step in the successor simulation, bringing the CFL number back within the stability limit. This can be done provided that the slices of data from the precursor simulations are reused, so that the inflow velocity conditions do not alter over several of the smaller time steps of the successor.

It was found that to bring the CFL number back within acceptable limits, the time step would

have to be decreased by a factor of about 16 in the successor simulation, leading to a very expensive simulation of the wake. It was known that this penalty arose from excessive cross-stream resolution downstream of the trailing edge, in a region where the high shear of the wall layers upstream had already been strongly diluted. To reduce the cost of the successor simulation, the cross-stream mesh was coarsened in this region, so that the time step in the successor simulation only needed to be a quarter of the time step in the precursor simulations.

2.8. Meshing

The computational mesh in the precursor simulation was identical with the finer of those used by Yang and Voke[20] for transition studies, while the boundary layer was produced by provoking an immediate transition of a Blasius boundary layer. The computational box was $460\vartheta_0 \times 23\vartheta_0 \times 15{\cdot}4\vartheta_0$, using the boundary layer momentum thickness ϑ_0 at the trailing edge in the wake simulation as a unit. The mesh was $255 \times 56 \times 48$. The slices of data used to define the inflow for the wake simulation were read from the 200th x-mesh plane, which is at a position $92\vartheta_0$ upstream of the outflow boundary layer simulation.

The mesh for the precursor simulation was uniform in both the x- and the z-direction but uniformly stretched in the y-direction, with a stretching ratio of 1.08. The smallest Δy nearest the wall was $0{\cdot}023\vartheta_0$, or about unity in wall units (ν/u_τ), and the largest value of Δy was $1{\cdot}8\vartheta_0$. Δx was $1{\cdot}8\vartheta_0$ and Δz was $0{\cdot}32\vartheta_0$.

In the successor simulation the computational mesh was stretched in both the x- and the y-direction, with the y-mesh corresponding to that used in the precursor over most of the top half of the domain, but with a symmetric mesh added to the bottom half of the domain. The computation box was $215\vartheta_0 \times 46\vartheta_0 \times 15{\cdot}4\vartheta_0$.

In the central region, close to the trailing edge and along the centreline of the wake, the precursor y-mesh was found to be too fine, resulting in an excessive reduction of the time step size to avoid Courant violations by the growing v in the near wake along the centreline. Eight control volumes close to the centreline were therefore merged in the successor simulation, both above and below the line of the plate, giving a total of 104 y-meshes in the successor simulation. Overall, the mesh was $127 \times 104 \times 48$. The streamwise mesh in the successor simulation was also compressed (with a mesh compression ratio of 1/1.05), from $\Delta x = 1{\cdot}8\vartheta_0$ down to $\Delta x = 0{\cdot}4\vartheta_0$ at the trailing edge which is $30\vartheta_0$ downstream of the inflow boundary, and maintained this resolution for a further $2\vartheta_0$. Thereafter the x-mesh stretched again with a stretching ratio of 1.03, reaching $\Delta x = 5{\cdot}7\vartheta_0$ at the outflow boundary of the successor wake simulation domain.

Since the Reynolds number was very low (Re_{ϑ_0} at the trailing edge was 908) no subgrid-scale model was included in this simulation.

3. RESULTS

3.1. The computations

Spatial dimensions are given in terms of ϑ_0 at the trailing edge. To convert to wall units, note that $\vartheta_0^+ = \vartheta_0 u_\tau/\nu = 44{\cdot}83$. Velocities are in terms of either u_τ or the free-stream velocity $U_e = 20u_\tau$ at the inflow plane, a little upstream of the trailing edge. The unit of time ϑ_0/u_τ is also convenient; the large-eddy lifetime in the boundary layer around the slicing plane, estimated as δ/u_τ, was $7{\cdot}7\vartheta_0/u_\tau = 345\nu/u_\tau^2$.

The time step in the precursor (boundary layer) simulation was $0{\cdot}003859\vartheta_0/u_\tau$ and in the successor (wake) simulation $0{\cdot}000969\vartheta_0/u_\tau$. Since the time step in the successor simulation was a

quarter the size of that used in the precursor simulation, each data slice was used as input four times without modification: the inflow velocities specified for the wake simulation did not alter for four time steps, being fixed to the values of the data slice corresponding to that time interval in the precursor simulation.

The boundary layer simulation was run for an extended period and had reached a statistically stationary state before data slicing was initiated. The data slices from the boundary layer simulation were gathered in advance. Data from temporally well-separated periods of the boundary layer simulation were used to provide uncorrelated boundary layer inflow specifications for the upper and lower halves of the inflow boundary of the wake simulation.

The wake simulation was started with zero flow throughout the computational volume: an impulsive acceleration was experienced at the first time step as the first data slice was imposed as inflow. The simulation was then run for 28,800 time steps (7200 inflow data slices or $27{\cdot}7\vartheta_0/u_\tau$) to allow the turbulent wake to become properly established. During this time the free-stream flow covered 5549_0 and therefore passed through the successor computational box about three times. It was considered that this was sufficient time for the turbulent wake to become established. The wake simulation was then continued for a further 67,200 time steps ($64{\cdot}69_0/u_\tau$), during which time the flow fields were sampled every 40 time steps. The statistics to be presented therefore include 1680 samples. The largest CFL numbers were about 0.23, the principal contribution to the CFL number coming from the v-component of velocity downstream of the trailing edge. The viscous number in these computations was very small. The error in the continuity was normally less than 10^{-10}, which is larger than the rounding accuracy for 64 bit computations only because of error accumulation in the cyclic reduction solver.

The simulation occupied 7.9 Mwords on a Cray XMP and each time step took 3.8 s of CPU time, rising to 4.5 s when the full statistical package, including computation of all Reynolds stress transport terms, was in operation. The computation of the statistics occupied 16% of the computer usage, but since it was only being performed every 40 time steps, it is clear that this aspect of the simulation was very expensive. The complete simulation of the wake required 115 h of CPU time. The precursor simulation of the boundary layer required an additional 40 h of CPU time, excluding prior study and conditioning of the boundary layer simulation. The sustained processing rate of the code was over 100 Mflops and the total number of floating point operations involved was of the order of 5×10^{13}.

3.2. Test of the code

The code was tested by imposing Blasius profiles at the inlet plane and observing the subsequent development of a Von Kármán vortex street (Figure 2). This allowed a check to be made of the innovative aspects of the computation, including outflow and stress-free boundary conditions and the method of imposing inflow conditions. The mesh was 31×64 and the computation box was eight times longer than its height. The third dimension was also computed but no three-dimensionality was detected in the resulting flow. At the trailing edge the Reynolds number based on momentum thickness, Re_{ϑ_0}, was 305, Re_d was 800 and Re_x was 211,000 for the test run discussed below.

Regularly spaced vortices alternating above and below the centreline developed in this test simulation. The ratio between the horizontal separation of vortices on the same side and the separation between the upper and lower vortices is close to 7, compared with a corresponding ratio of about 5 found in the photographs of Heinemann *et al.*[23] The estimation of the Strouhal number S of the vortex street is complicated by the absence of a natural length scale associated with the generation of the vortices; the plate thickness is nominally zero and the smallest

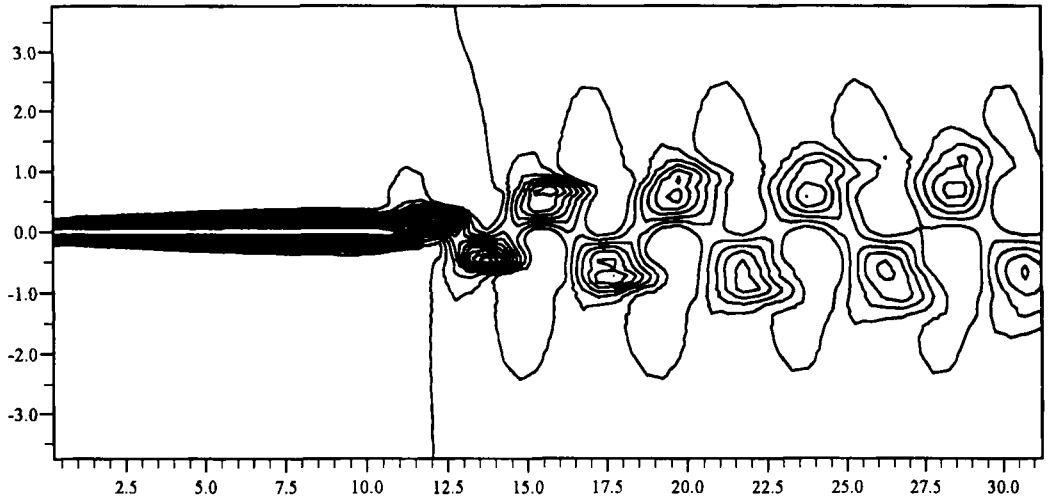

Figure 2. A typical simulated liminar wake showing the vortex street in the form of contours of streamwise velocity

cross-stream mesh spacing is unlikely to be the important governing length scale, being very much smaller than the integral length scales of the laminar boundary layer. Basing the Strouhal number on twice the thickness of the boundary layer at the trailing edge, 2δ, we find $S = 2\delta n/U_e = 0.21$, which is very similar to the values quoted by Heinemann *et al.*[23] at similar Reynolds numbers and low Mach numbers. Basing the Strouhal number on the initial displacement thickness of the wake, which is perhaps more realistic, give lower values of S around 0.07. We have assumed the n/U_e is equal to the streamwise spacing of the same-side vortices.

3.3. Integral parameters

The precursor turbulent boundary layers were produced by specifying a Blasius profile at the inlet plane close to the surface, overlaid with a high level of pseudorandom disturbance in the free stream, in the manner reported by Yang and Voke.[18] The high level of free stream disturbance produced an immediate transition to turbulence in the boundary layer. The integral characteristics of the layer move towards those expected in a young turbulent boundary layer, with a typical turbulent shape factor, friction coefficient and growth rate. The free stream disturbances decay rapidly at first, then more slowly as the physical correlations of decaying grid turbulence are established. At the slicing plane the free-stream turbulence level u'/U_e is less than 1%.

In the wake simulation the momentum thickness grows slowly up to the trailing edge, as we expect. At the trailing edge the momentum thickness Reynolds number $Re_{\vartheta_0} = 908$. The wake simulation beyond the trailing edge covers a steamwise distance of $180\vartheta_0$, which corresponds to a distance well beyond the near wake as defined by Ramaprian *et al.*[24] and into the intermediate wake which they assume extends from $x = 25\vartheta_0$ to about $x = 350\vartheta_0$. It does not reach the far-wake region in which the wake has forgotten its origin and achieved an asymptotic state.

Since neither simulation allowed flow through the side boundaries, a small pressure gradient exists which changes the outer flow. In the boundary layer simulation this results in an increase in the outer flow velocity as the displacement thickness of the boundary layer increases, corresponding to a small favourable pressure gradient. In the wake the displacement thickness

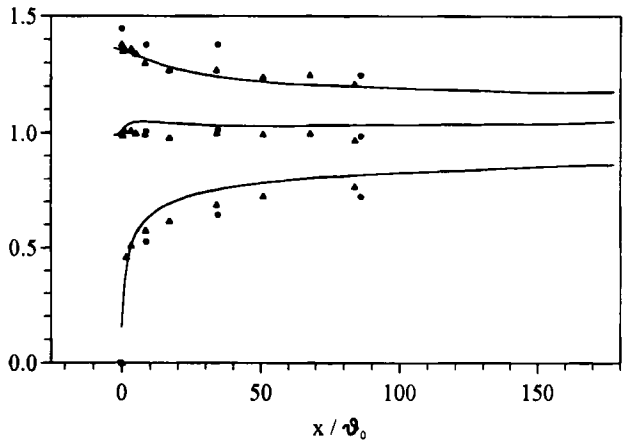

Figure 3. Shape factor δ^*/ϑ_0 (upper curve), momentum thickness ϑ/ϑ_0 (middle curve) and centreline velocity U_c/U_e (lower curve) of the wake. Lines, present results; circles, Chevray and Kovasnay;[25] triangles, Andreopoulos and Bradshaw[26]

of the inner flow declines as the wake fills in and the outer flow decelerates under the influence of a small adverse pressure gradient.

The Reynolds number based on momentum thickness at the trailing edge, Re_{ϑ_0}, was about 900 and hence lower than that of the available experimental data, which cover a range of Re_{ϑ_0} above 1500. We have made comparisons with Chevray and Kovasnay[25] whose measurements were at $Re_{\vartheta_0} = 1580$ and with Andreopoulos and Bradshaw[26] at $Re_{\vartheta_0} = 13600$.

In a normal free wake the displacement thickness alters but the absence of any free-stream pressure gradient or other forces beyond the trailing edge ensures that the momentum thickness is constant there. We find that the momentum thickness ϑ in the simulation increases noticeably just beyond the trailing edge (Figure 3), rising by about 4% over a distance of the order of $5\vartheta_0$. It roughly maintains this level over the remainder of the wake simulation. The reasons for the initial rise just beyond the trailing edge are discussed below. The shape factor $H = \delta^*/\vartheta$ behaves just as expected in the wake (Figure 3), its decline agreeing well with experiments at higher Reynolds numbers. The third curve in Figure 3, showing the growth of the centreline velocity, suggests that our simulated wake fills in rather more rapidly than the experiments at higher Reynolds numbers.

3.4. Mean flow characteristics

The mean streamwise, normal and spanwise velocities are referred to as U, V and W respectively. The U-profiles shown in Figure 4 at stations corresponding to those of Chevray and Kovasnay[25] are qualitatively very similar to those found experimentally. Because the rate at which the centreline velocity fills in is different from that found by either Andreopoulos and Bradshaw[26] or Chevray and Kovasnay,[25] we have not overlaid their experimental points on these graphs. A detailed investigation of the behaviour of the mean U in the inner boundary layer and near wake[27] shows that the overall behaviour of U is as expected, with a rapid rise in U as the skin friction vanishes at the trailing edge. A small but distinct ridge in the streamwise velocity occurs around the transverse plane passing through the trailing edge; the increment is quite small compared with the free-stream velocity. It dies out completely in the far field. To understand the origin of this ridge, we must also look at the mean V and pressure fields.

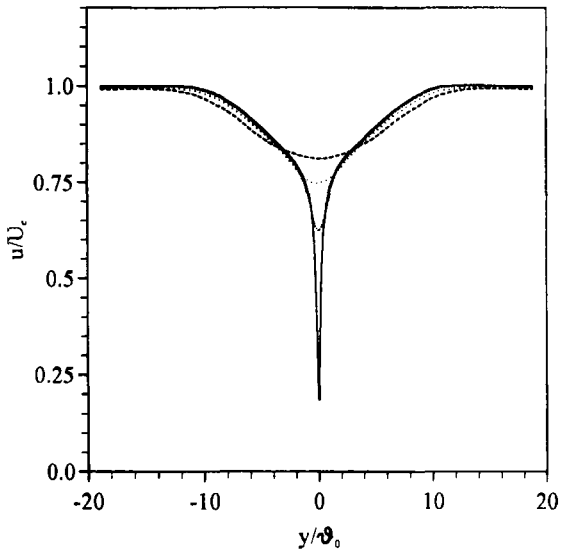

Figure 4. Profiles of mean streamwise velocity U/U_e at $x/\vartheta_0 = 0$ (solid), 9 (close dotted), 34 (wide dotted) and 87 (dashed)

The rapid rise in U just beyond the trailing edge of the plate is the dominant feature driving the behaviour of the flow in that region. The large positive value of $\partial U/\partial x$ must give rise to a corresponding negative value of $\partial V/\partial y$; this is confirmed by the simulation. The normal velocity V is zero on the intruding plate and grows away from the plate in the boundary layer, being slightly negative for $y < 0$ and positive for $y > 0$. In the wake this pattern is reversed, with the decreasing displacement thickness pulling flow inwards; V is slightly positive for $y < 0$ and negative for $y > 0$. At the trailing edge the large positive $\partial U/\partial x$ produces an antisymmetric ridge in V, the peak V being 2% of U_e. Approaching the trailing edge, the flow therefore encounters a line of positive $\partial U/\partial x$ closely followed by a line of negative $\partial U/\partial x$: this is the origin of a small ridge in U coinciding with the position of the V ridge. The acceleration of U and the subsequent deceleration supply the mass flux for the inward V, which in turn supplies the mass flux required by the rapidly filling central wake. The mean W is very small, as we expect in a spanwise homogeneous mean flow: the above analysis therefore need only take account of U and V.

The inner wake fills in rapidly, because the shear induced by the wall produces a large turbulent transport of momentum towards the centreline. The resulting acceleration of the flow produces a region of very low pressure, sucking in the surrounding fluid to supply the increasing mass flux. The central region immediately downstream of the trailing edge acts rather like a mass sink in this respect. If the surrounding flow pattern were dictated entirely by mass conservation, we should see this reflected in the shape of the pressure field, whose gradient produces the required changes in U and V. The simulation indeed shows a definite increase in the favourable pressure gradient in the last $8\vartheta_0$ before the trailing edge and a rather more precipitate adverse gradient as the pressure recovers in the first $8\vartheta_0$ before the trailing edge, at least off the centreline: the recovery is much slower along the centre of the wake. The lowest pressure occurs fractionally before the trailing edge, on the surface of the plate.

The striking pattern of the pressure field accords with the analysis given above of the mean flow in the central region and close to the trailing edge. There is a hole in P, aligned with the V ridge, which dies out progressively in the far field and produces net flow towards the plane of the trailing edge and inwards. It is interesting to note that the pressure field opposes the

infilling of the inner wake, which is evidently due solely to turbulent and viscous momentum transport induced by the mean shear.

The strong adverse pressure gradient occurs in the same x-interval as the 4% increase in momentum thickness. The other forces act merely to redistribute momentum, since downstream of the trailing edge they cannot create or destroy it. The adverse pressure gradient, however, produced an overall loss of momentum even while the centre of the wake is rapidly filling in. It is therefore possible for the momentum thickness to increase while the displacement thickness is falling.

3.5. Turbulence characteristics

The u'-profiles (Figure 5) reveal one source of disagreement in comparing the simulation results with the experiments. The intensity does not fall to zero in the free stream owing to the presence of residual free-stream turbulence from the precursor simulation. A side-effect of this which is of greater significance than the small free-stream level itself in the spread in the main intensity profiles, which extend out beyond $y = 10\vartheta_0$, even for the lower values of x/ϑ_0. The U-profiles in Figure 4 do show a slight spread beyond $y = 10\vartheta_0$, but the difference is more obvious for the fluctuation; our u' at $y = 10\vartheta_0$ is over 2% of U_e, rising to over 3% at the streamwise position $x = 87\vartheta_0$, while the experimental measurements of Chevray and Kovasnay[25] show values of about 1% and hardly any rise even at their $x = 86\vartheta_0$ station. The peaks in the u'-profiles move away from the centreline as we move downstream in a familiar manner, but in general we find the positions of the peaks systematically further from the centreline than the peaks in the measurements of Chevray and Kovasnay.[25] The exception is at the $x = 34\vartheta_0$ station, where both the position and magnitude of the peak agree well.

Not all the features of importance are picked up by these graphs. Detailed study[27] of the u intensity reveals two 'horns' occurring just downstream of the trailing edge, representing an increase in u'^2 of about 10%. They are neatly aligned with the peaks in the boundary layer intensity profiles and with the plane of the trailing edge, but their influence extends out beyond $y = \pm 2\vartheta_0$ and some distance downstream. The peak value of u'^2 is almost $10u_\tau^2$ very close to

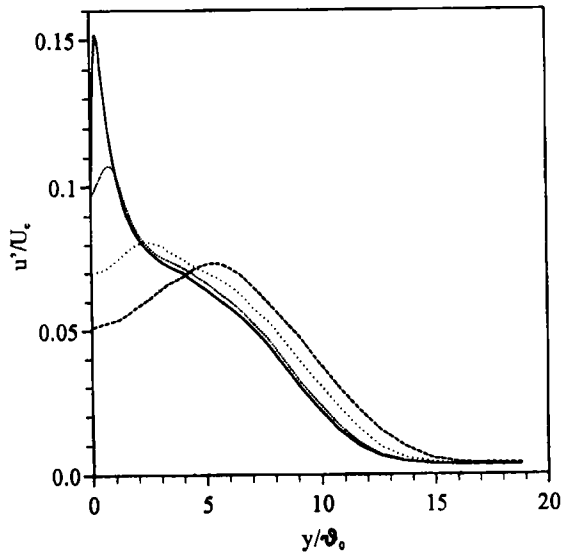

Figure 5. Profiles of RMS fluctuation u'/U_e at $x/\vartheta_0 = 0$, 9, 34 and 87 (as Figure 3)

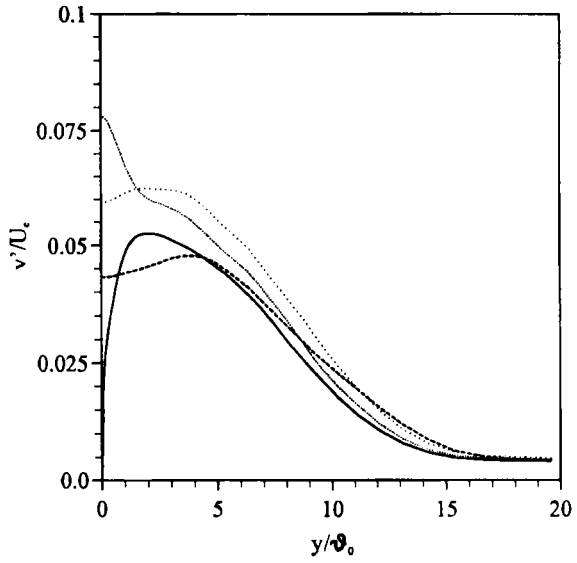

Figure 6. Profiles of RMS fluctuation v'/U_e at $x/\vartheta_0 = 0$, 9, 34 and 87 (as Figure 3)

the centreline and $0{\cdot}75\vartheta_0$ downstream of the trailing edge. The presence of the horns strongly suggests that in spite of the nominally zero thickness of the plate, some form of shedding is taking place from the trailing edge.

The v'-profiles in Figure 6 show still more interesting features. In contrast with the experimental profiles, the simulation has a sharp rise in v' as we pass the trailing edge, and for the $x = 9\vartheta_0$ curve a distinct central peak seems to be superimposed. As with the u'-profiles, the v'-profiles all fall slowly and the level at $y = 10\vartheta_0$ is about 2%. The free-stream value is clearly non-zero. In general the fluctuation levels are higher than those found experimentally. More detailed study shows a striking central peak in v'^2 overriding the normal central trough of v'^2 in a small region immediately downstream of the trailing edge. The maximum value of v'^2 is $4{\cdot}5u_\tau^2$ $2\vartheta_0$ downstream of the trailing edge. It is hard to believe that this rapid rise in v' from a zero value in such a short distance is unconnected with the horns in the u intensity in the same locality, again suggesting that shedding is taking place.

The lateral intensity level w'^2 is slightly lower, the largest value of w'^2 being $2{\cdot}8u_\tau^2$ at the same streamwise location as the v'^2 peak, but with a suggestion of enhancement off the centreline. The actual peaks (not shown) are the same distance from the centreline as the u'^2 horns. Clearly there is coupling between these phenomena found in the three velocity fluctuations close to the separation point. Further study will be required to understand fully the interactions between the three components, but the data presented here suggest that three-dimensional shedding is taking place in a small region just downstream of the trailing edge. This hypothesis is supported by vector plots of the instantaneous u' fluctuations in the same region (Figure 7).

The picture that is emerging of a region of high turbulent activity, partially coherent in nature, just beyond the trailing edge is supported by the initial analysis of the Reynolds stress transport. The terms in the transport equation for τ_{12} have been computed approximately. These terms are higher-order and tend to require longer periods of sampling to obtain adequate statistical convergence. Also, owing to the staggered mesh used for the simulation, the correct definition of the algorithm for computing most of the terms is ambiguous: we have interpolated

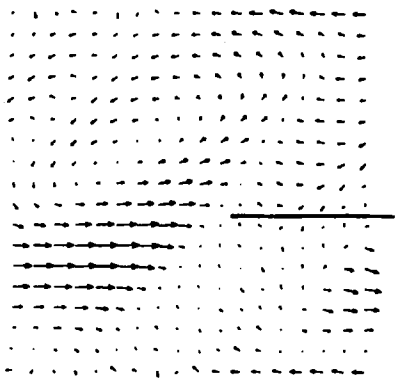

Figure 7. An instantaneous fluctuating flow field: vectors of (u', v'). The region $x = 3{\cdot}48$ to $4{\cdot}45$, $y = -0{\cdot}038$ to $0{\cdot}027$, $z = 1{\cdot}0$ is shown stretched so that the meshes are evenly distributed. The solid line is the trailing edge

all three velocities and the velocity gradients to the centre of the mass/pressure cells before computing the terms, which is a straightforward approach though it cannot reproduce the precise balance of the analytic transport equation. A residual term is present representing interpolation and differing errors, which cannot be interpreted as part of any of the individual terms. This error is quite low over most of the domain, but unfortunately has large peaks in the region that is the primary focus of interest just downstream of the trailing edge. Details of the behaviour of the terms, including the error term, are given in Reference 27.

The convective transport has a peak just downstream of the trailing edge, but the overall contribution from this term is not large. The diffusive transport is very much larger and shows a highly localized antisymmetric peak very close to the trailing edge. The peaks are comparable in size with the diffusive transport in the boundary layer upstream and of the same sign. This is not unexpected, since the instability giving rise to the shedding produces a large negative u-gradient of τ_{12} across the centreline in a region of strong turbulent activity. The sudden disappearance of the plate as the flow passes the trailing edge results in these adjacent regions of opposite τ_{12} being brought into contact.

The production of stress in the region is concentrated into a shallow pair of antisymmetric peaks aligned with the position of the maxima of turbulent fluctuations. The pressure strain term is of particular interest. The antisymmetric pattern in the boundary layer upstream is reversed in the region of the shedding, though the inverted peaks are less sharp than was the case for the diffusive transport. The peak value is large enough to represent an important contribution to the stress balance in a small region in the near wake, though there is some doubt as to the reality of the reversal of the pressure strain, since it no longer balances the large diffusive transport. The mismatch between the two is accounted for by the error term. Since the computation of the pressure strain and the pressure part of the diffusive transport terms involves a number of ambiguous interpolations, it is likely that the errors necessarily generated in computing them contribute significantly to the overall imbalance.

The viscous dissipation of Reynolds stress τ_{12} is also found to peak in the same way in two antisymmetric lobes centred on the positions of maximum stress. The numerical values of the peaks are hardly larger than those in the boundary layer. We find that there is a rough balance between the production and viscous dissipation in the very near wake where we suppose shedding to be taking place, in contrast with the situation in the boundary layer where the viscous dissipation close to the wall is larger than the production and is fed by the transport terms.

It is evident that the principal Reynolds stress just beyond the trailing edge is being produced locally, at the same time as it is being transported by diffusion and is being redistributed into other components of the Reynolds stress. It is difficult to draw firm conclusions because of the errors involved in computing these types of quantities from staggered velocity components, errors which unfortunately appear to be most severe in the region of the shedding; a method of extracting more reliable estimates of transport terms in these simulations is the subject of current research.

4. CONCLUSIONS

The numerical techniques introduced to allow the simulation of the turbulent wake behind a flat plate appear to have been very successful. We have devised methods for transferring turbulence data from one simulation to another with a different mesh distribution and for dealing in an efficient though approximate way with an intruding solid trailing edge within a simulation. We have also developed, tested and utilized in the simulation advective boundary conditions. All these techniques appear to have potential for further development and use.

A laminar test run produced a Von Kármán vortex street very similar to those found experimentally. The simulated turbulent wake has many of the statistical characteristics observed experimentally at similar or higher Reynolds numbers, apart from effects arising from the presence of some residual free-stream turbulence in the simulation. We also observe that the simulated turbulent wake fills in more rapidly along the centreline just beyond the trailing edge than the experimental wakes. Some evidence has been presented that indicates that three-dimensional shedding is taking place from the trailing edge in a small region just downstream. This gives rise to some striking patterns of peaks in the turbulence intensities and stress transport terms.

Current work aims to improve upon the results reported here by performing a simulation using inflow boundary layer data whose credibility is assured through close agreement with experiment. Higher mesh resolution, together with an appropriate subgrid-scale model, should give further confidence in the accuracy of the simulation. A method is under development for computing terms in balance equations that guarantees that the sum of the terms tends to zero in the limit as the number of statistical samples increases.

ACKNOWLEDGEMENTS

This work was supported by the U.K. Ministry of Defence and the Department of Trade and Industry under contract 2042/87/XR/Aero. The supercomputer resources were supplied by the Science and Engineering Research Council under grants GR/E 75479 and GR/F 89596. This work was performed while the authors were employed by Queen Mary and Westfield College, University of London.

REFERENCES

1. J. H. Chen, B. J. Cantwell and N. N. Mansour, 'Direct numerical simulations of a plane compressible wake: stability, vorticity dynamics and topology', *Rep. TF-46*, Department of Mechanical Engineering, Stanford University, 1989.
2. S. K. Lele, 'Direct numerical simulation of compressible free shear flows', *AIAA-889-0374*, 1989.
3. P. Compte, Y. Fouillet, M. A. Gonze, M. Lesieur, O. Métais and X. Normand, 'Generation of coherent structures in free shear layers', in O. Métais and M. Lesieur (eds), *Turbulence and Coherent Structures*, Kluwer, Dordrecht, 1991, pp. 45–73.

4. D. K. Lilly, 'On the computational stability of numerical solutions of time-dependent, non-linear geophysical fluid dynamics problems', *Mon. Weather Rev.*, **93**, 11–26, 1965.
5. A. Arakawa, 'Computational design for long-term numerical integration of the equations of fluid motion: two-dimensional incompressible flow', *J. Comput. Phys.*, **1**, 119–143, 1966.
6. K. Bryan, 'A scheme for numerical integration of the equations of motion on an irregular grid free of nonlinear instability', *Mon. Weather Rev.*, **94**, 39–40, 1966.
7. J. Smagorinsky, 'General circulation experiments with the primitive equations: Part I, The basic experiment', *Mon. Weather Rev.*, **91**, 99–164, 1963.
8. J. W. Deardorff, 'A numerical study of three-dimensional turbulent channel flow at large Reynolds numbers', *J. Fluid Mech.*, **41**, 453–480, 1970.
9. U. Schumann, 'Subgrid scale model for finite difference simulations of turbulent flows in plane channels and annuli', *J. Comput. Phys.*, **18**, 376–401, 1975.
10. G. Grötzbach, 'Application of the TURBIT-3 subgrid scale model to scales between large eddy and direct simulation', in U. Schumann and R. Friedrich (eds), *Notes on Numerical Fluid Mechanics*, Vol. 15, *Direct and Large Eddy Simulation of Turbulence*, Vieweg, Braunschweig, 1986, pp. 210–226.
11. P. J. Mason, 'Large-eddy simulation of the convective atmospheric boundary layer', *J. Atmos. Sci.*, **46**, 1989.
12. H. Klein and R. Friedrich, 'Manipulating large-scale turbulence in a channel and a boundary layer', *Seventh Symp. on Turbulent Shear Flows*, Stanford, 1989, Paper 25-4.
13. S. Gao, D. C. Leslie and P. R. Voke, 'Large eddy simulation of thermal impinging jets', *Rep. ME-FD/91.02*, Department of Mechanical Engineering, University of Surrey, Guildford, 1991.
14. T. Gertz, U. Schumann and S. E. Elgobashi, 'Direct numerical simulation of stratified homogeneous shear flows', *J. Fluid Mech.*, **200**, 536–594, 1989.
15. S. Gavrilakis, 'Numerical simulation of low-Reynolds-number turbulent flow through a straight square duct', *J. Fluid Mech.*, **244**, 101–129, 1992.
16. P. N. Schwarztrauber, 'A direct method for the discrete solution of separable elliptic equations', *SIAM J. Numer. Anal.*, 11, 1136–1150, 1974.
17. H. M. Tsai, P. R. Voke and D. C. Leslie, 'Large-eddy simulation of turbulent free shear flows', in C. Taylor, W. G. Habashi and M. M. Hafez (eds), *Numerical methods in Laminar and Turbulent Flows V*, Peneridge, Swansea, 1987, pp. 363–373.
18. Z. Y. Yang and P. R. Voke, 'Numerical simulation of transition in the presence of free-stream turbulence', in O. Pironneau, W. Rodi, I. L. Ryhming, A. M. Savill and T. V. Truong (eds), *Numerical Simulation of Unsteady Flows and Transition to Turbulence*, Cambridge University Press, New York, 1992, pp. 398–403.
19. A. Bottaro, 'Note on open boundary condition for elliptic flows', *Numer. Heat Transfer B*, **18**, 243–256, 1990.
20. Z. Y. Yang and P. R. Voke, 'Numerical simulation of transition under turbulence, *Rep. ME-FD/91.01*, Department of Mechanical Engineering, University of Surrey, Guildford, 1991.
21. S. H. Lo, 'Pattern recognition analysis of organised eddy structures in a numerically simulated turbulent plane jet', *Ph.D. Thesis*, Department of Aeronautical Engineering, Queen Mary and Westfield College, University of London, 1993.
22. P. Moin and J. Kim, 'On the numerical solution of time-dependent viscous incompressible fluid flows involving solid boundaries', *J. Comput. Phys.*, **35**, 381–392, 1980.
23. H. J. Heinemann, O. Lawaczeck and K. A. Bütefisch, 'Kármán vortices and their frequency determination in the wakes of profiles in the subsonic and transonic regime', *Symp. Transonicum II*, Göttingen, 1975, Springer, Berlin, 1976, pp. 75–82.
24. B. R. Ramaprian, V. C. Patel and M. S. Sastry, 'The symmetric turbulent wake of a flat plate', *AIAA J.*, **20**, 1228–1235, 1982.
25. R. Chevray and L. S. G. Kovasnay, 'Turbulence measurements in the wake of a thin flat plate', *AIAA J.*, **7**, 1641–1643, 1969.
26. J. Andreopoulos and P. Bradshaw, 'Measurements in interacting turbulent shear layers in the near wake of a flat plate', *J. Fluid Mech.*, **100**, 639–668.
27. S. G. Potamitis and P. R. Voke, 'Numerical simulation of a plane wake', *Rep. ME-FD/92.04*, Department of Mechanical Engineering, University of Surrey, Guildford, 1992.